Transport and Magnetic Properties of the Perovskites $La_{1-y}MnO_3$ and $LaMn_{1-z}O_3$

J. Töpfer* and J. B. Goodenough

Center for Materials Science and Engineering, ETC 9.102, University of Texas at Austin, Austin, Texas, 78712

Received January 3, 1997. Revised Manuscript Received April 15, 1997[⊗]

Single-phase samples of $La_{1-y}MnO_{3-(3y/2)+\delta}$ with $0 \le y \le 0.09$ and $LaMn_{1-z}O_{3-(3z/2)+\delta}$ with $0 \le z \le 0.09$ have been prepared via the citrate method with subsequent heating at different temperatures and partial pressures of oxygen. Oxygen parameters $0 \le \delta \le 0.18$ were obtained. At room temperature, all compositions y and z have the orthorhombic structure of $GdFeO_3$ (*Pbnm*) for small values of δ and the rhombohedral structure of $LaAlO_3$ ($R\bar{3}c$) for larger values of δ. Below a temperature T_c, all samples show a weak ferromagnetism at $\delta = 0$ that increases with δ, samples with $y = 0$ approaching a full ferromagnetic alignment of all Mn moments in the range $0.10 < \delta < 0.13$. At smaller δ, the orthorhombic samples contain randomly distributed superparamagnetic clusters that couple via an antiferromagnetic matrix to form a spin glass below T_c. At higher values of δ, a sharp increase of T_c to a value greater than the Weiss temperature θ_p for the paramagnetic phase indicates a first-order transition on lowering T through T_c from a polaronic to an itinerant-electron conductor within the matrix between trapped-hole clusters; lack of full ferromagnetic alignment of the Mn spins is found despite the higher value of T_c. Transport properties show an increasing trapping out of mobile polaronic holes on cooling to T_c with a release of these holes below T_c. Samples with $z > 0$ trap out mobile holes more strongly and remain polaronic at all temperatures except below T_c at highest values of δ in the matrix between hole-rich clusters.

Introduction

Extensive studies have been made of the manganese-oxide perovskites $Ln_{1-x}A_xMnO_3$ with Ln = rare-earth atoms and A = Ca, Sr, or Ba especially in the past three years after the discovery of giant magnetoresistance in these compounds.[1−3] This in turn has created renewed interest in the properties of the nonstoichiometric compound $LaMnO_{3+\delta}$.[4−6] It was recognized early[7,8] that stoichiometric $LaMnO_3$ is approached only by firing at lower partial pressures of oxygen; firing in air, e.g., at 1200 °C, yields $LaMnO_{3+\delta}$ with $\delta \approx 0.05$. Later it was shown that the nonstoichiometry δ is accommodated as cation vacancies at high oxygen partial pressure.[9−11] Therefore the composition of $LaMnO_{3+\delta}$ is better expressed as $La_{1-\epsilon}Mn_{1-\epsilon}O_3$ with $\epsilon = \delta/(3+\delta)$ or

$$LaMn^{3+}_{1-2\delta}\,Mn^{4+}_{2\delta}O_{3+\delta} = (3+\delta)/3La_{3/(3+\delta)}\square_{\delta/(3+\delta)}Mn^{3+}_{(3-6\delta)/(3+\delta)} \times Mn^{4+}_{6\delta/(3+\delta)}\square_{\delta/(3+\delta)}O_{3.00} \quad (1)$$

A nonstoichiometric cation ratio La/Mn < 1 and its influence on structure and high-temperature conductivity have been reported by Takeda et al.,[12] and a complete phase diagram of the La−Mn−O system has shown a small range of solid solubility on both sides of the ratio La/Mn = 1.[13] The preparation of a thin-film sample of $La_{1-y}MnO_3$ with $y \approx 0.3$ by pulsed laser deposition has been reported.[14] Very recently, after the completion of this study a report on the structure, transport and magnetic properties of perovskites with different values of y and z ($0 \le y \le 0.2$; $0 \le z \le 0.2$) prepared at the same temperature and thus having similar values of δ appeared.[15]

In a preceding paper, we have proposed a tentative low-temperature phase diagram for the system $LaMnO_{3+\delta}$ and interpreted the physical properties observed.[5] Here we extend this study to include the nonstoichiometric materials with La/Mn ≠ 1. We report on the magnetic and electrical properties of the systems

* To whom correspondence should be addressed. Present address: Hermsdorfer Institut für Technische Keramik, Naumburger Strasse, 07629 Hermsdorf, Germany.

[⊗] Abstract published in *Advance ACS Abstracts,* June 1, 1997.

(1) von Helmolt, R.; Wecker, J.; Holzapfel, B.; Schultz, L.; Sammer, K. *Phys. Rev. Lett.* **1993**, *71*, 2331.
(2) Urushibara, A.; Moritomo, Y.; Arima, T.; Asamitsu, A.; Kido, G.; Tokura, Y. *Phys. Rev. B* **1995**, *51*, 14103.
(3) Chahara, K.; Ohno, T.; Kasai, M.; Kozono, Y. *Appl. Phys. Lett.* **1993**, *63*, 1990.
(4) Mahendiran, R.; Tawary, S.; Raychaudhuri, K.; Ramakrishnan, T. V.; Mahesh, R.; Rangarvittal, N.; Rao, C. N. R. *Phys. Rev. B* **1996**, *53*, 3348.
(5) Töpfer, J.; Goodenough, J. B. *J. Solid State Chem.*, in press.
(6) Cheetham, A. K.; Rao, C. N. R.; Vogt, T. *J. Solid State Chem.* **1996**, *126*, 337.
(7) Wold, A.; Arnott, R. J. *J. Phys. Chem. Solids* **1959**, *9*, 176.
(8) Kamata, K.; Nakajima, T.; Hayashi, T.; Nakamura, T. *Mater. Res. Bull.* **1978**, *13*, 49.
(9) Kuo, J. H.; Anderson, H. U.; Sparlin, D. M. *J. Solid State Chem.* **1989**, *83*, 52.
(10) van Roosmalen, J. A. M.; Cordfunke, E. H. P. *J. Solid State Chem.* **1994**, *110*, 100.
(11) Töpfer, J.; Dieckmann, R., manuscript in preparation.
(12) Takeda, Y.; Nakai, S.; Kojima, T.; Kanno, R.; Imanishi, N.; Shen, G.; Yamamoto, O.; Mori, M.; Asakawa, C.; Abe, T. *Mater. Res. Bull.* **1991**, *26*, 153.
(13) van Roosmalen, J. A. M.; van Vlaanderen, P.; Cordfunke, E. H. P.; Ijdo, W. L.; Ijdo, D. J. W. *J. Solid State Chem.* **1995**, *114*, 516.
(14) Sundar Manoharan, S.; Kumar, D.; Hegde, M. S.; Satyalakshmi, K. M.; Prasad, V.; Subramanian, S. V. *J. Solid State Chem.* **1995**, *117*, 420.
(15) Arulraj, A.; Mahesh, R.; Subbanna, G. N.; Mahendiran, R.; Raychaudhuri, A. K.; Rao, C. N. R. *J. Solid State Chem.* **1996**, *127*, 87.

S0897-4756(97)00021-5 CCC: $14.00

Table 1. Preparation Conditions: 24 h 1200 °C Ar (a), 24 h 1200 °C Air (b), 48 h 800 °C O_2 (c), Directly 100 h 800 °C O_2 (d); Nonstoichiometry Parameter δ (±0.01) As Determined by Chemical Titration; Composition of Samples Calculated on the Basis of δ Values; Lattice Parameters (*a*, *b*, *c* for Orthorhombic Samples and *a*, α for Rhombohedral Samples); Effective Magnetic Moments from Curie−Weiss Part of χ vs *T* Curves (200−320 K); and Spin-Only Magnetic Moment for Samples of the Systems $La_{1-y}MnO_{3-(3y/2)+\delta}$ and $LaMn_{1-z}O_{3-(3z/2)+\delta}$

T	δ	composition	*a* (Å)	*b* (Å)	*c* (Å)	α (deg)	μ_{eff}	μ_{so}
			(I) $La_{1-y}MnO_{3-(3y/2)+\delta}$					
			(1) $y = 0.00$; $LaMnO_{3+\delta}$					
a	0.00	$LaMnO_{3.00}$	5.532(4)	5.738(1)	7.693(5)		5.55	4.90
b	0.05	$La^{3+}_{0.984}Mn^{3+}_{0.885}Mn^{4+}_{0.098}O_{3.00}$	5.537(2)	5.656(2)	7.715(3)		6.19	4.81
c	0.11	$La^{3+}_{0.965}Mn^{3+}_{0.752}Mn^{4+}_{0.212}O_{3.00}$	5.472(1)			60.68(1)	5.49	4.61
d	0.18	$La^{3+}_{0.943}Mn^{3+}_{0.604}Mn^{4+}_{0.340}O_{3.00}$	5.471(2)			60.54(1)	4.86	4.43
			(2) $y = 0.05$; $La_{0.95}MnO_{2.925+\delta}$					
a	0.01	$La^{3+}_{0.950}Mn^{3+}_{0.990}Mn^{4+}_{0.010}O_{2.93}$	5.532(1)	5.711(1)	7.698(1)		5.72	4.89
b	0.05	$La^{3+}_{0.950}Mn^{3+}_{0.900}Mn^{4+}_{0.100}O_{2.97}$	5.543(1)	5.589(1)	7.743(1)		6.14	4.81
c	0.14	$La^{3+}_{0.931}Mn^{3+}_{0.706}Mn^{4+}_{0.274}O_{3.00}$	5.471(1))			60.65(1)	6.61	4.59
d	0.16	$La^{3+}_{0.925}Mn^{3+}_{0.662}Mn^{4+}_{0.312}O_{3.00}$	5.479(3)			60.53(1)	3.2	4.54
			(3) $y = 0.09$; $La_{0.91}MnO_{2.865+\delta}$					
a	0.00	$La^{3+}_{0.910}Mn^{3+}_{1.000}O_{2.86}$	5.529(1)	5.698(1)	7.697(1)		5.56	4.90
b	0.06	$La^{3+}_{0.910}Mn^{3+}_{0.880}Mn^{4+}_{0.120}O_{2.92}$	5.535(3)	5.554(2)	7.770(3)		6.24	4.79
c	0.12	$La^{3+}_{0.910}Mn^{3+}_{0.760}Mn^{4+}_{0.240}O_{2.98}$	5.475(1)			60.55(1)	6.65	4.68
d	0.14	$La^{3+}_{0.910}Mn^{3+}_{0.720}Mn^{4+}_{0.280}O_{3.00}$	5.470(3)			60.48(1)	4.9	4.64
			(II) $LaMn_{1-z}O_{3-(3z/2)+\delta}$					
			(2) $z = 0.05$; $LaMn_{0.95}O_{2.925+\delta}$					
a	0.04	$La^{3+}_{1.000}Mn^{3+}_{0.870}Mn^{4+}_{0.080}O_{2.96}$	5.533(1)	5.684(1)	7.718(2)		5.59	4.70
b	0.08	$La^{3+}_{1.000}Mn^{3+}_{0.790}Mn^{4+}_{0.160}O_{3.00}$	5.533(1)	5.608(2)	7.753(2)		5.65	4.62
c	0.16	$La^{3+}_{0.974}Mn^{+}_{0.614}Mn^{4+}_{0.312}O_{3.00}$	5.467(1)			60.72(1)	6.26	4.41
d	0.19	$La^{3+}_{0.965}Mn^{3+}_{0.550}Mn^{4+}_{0.366}O_{3.00}$	5.478(2)			60.36(2)	4.5	4.32
			(3) $z = 0.09$; $LaMn_{0.91}O_{2.865+\delta}$					
a	0.03	$La^{3+}_{1.000}Mn^{3+}_{0.850}Mn^{4+}_{0.060}O_{2.89}$	5.534(1)	5.710(1)	7.705(1)		5.35	4.62
b	0.10	$La^{3+}_{1.000}Mn^{3+}_{0.710}Mn^{4+}_{0.200}O_{2.96}$	5.529(2)	5.560(2)	7.775(3)		5.73	4.48
c	0.16	$La^{3+}_{0.993}Mn^{3+}_{0.586}Mn^{4+}_{0.318}O_{3.00}$	5.461(4)			60.62(3)	5.76	4.34
d	0.18	$La^{3+}_{0.987}Mn^{3+}_{0.543}Mn^{4+}_{0.355}O_{3.00}$	5.467(4)			60.67(4)	5.2	4.29

$La_{1-y}MnO_{3-(3y/2)+\delta}$ with $0 \le y \le 0.09$ and $LaMn_{1-z}O_{3-(3z/2)+\delta}$ with $0 \le z \le 0.09$ with different values of δ for each particular composition *y* and *z* and discuss the inpact of the nonstoichiometry δ on the crystal structure, transport, and magnetic properties.

Experimental Section

The samples were prepared by dissolving La_2O_3 (dried at 950 °C before use) and $MnCO_3$ (Mn content gravimetrically determined) in acetic acid. A few crystals of hydroxyl aminochloride were added in order to obtain a clear solution free of higher-valent Mn ions. Then a solution of citric acid was added, and a white precipitate was obtained. The solution was slowly evaporated on a hot plate, and the obtained solid was calcined at 800 °C. Pellets of the precursor powders were pressed and fired at 1300 °C for 24 h in air. After grinding and repelletizing, the heat treatment at 1300 °C for 24 h in air was repeated. Final equilibration runs were performed at 800 and 1200 °C under an atmosphere of argon, air, or oxygen. The samples fired in argon or oxygen were slowly cooled in the furnace in the gas atmosphere; those heated in air were quenched. To increase the concentrations of Mn^{4+}, a set of samples was prepared by direct heating of pellets of the precursor powder at 800 °C in oxygen. Due to the low temperature of this synthesis route, the density of these samples was much lower than that of the sample sets prepared by prefiring at 1300 °C.

Powder X-ray diffraction was performed with Cu Kα radiation and Si as internal standard. The nonstoichiometry parameter δ was determined by chemical titration: the samples were dissolved in an excess of 0.1 N VO^{2+} in sulfuric acid and potentiometrically titrated with 0.1 N $KMnO_4$ solution (calculation of δ based on the nominal cationic composition). This method was checked with Mn_3O_4 to give $Mn_3O_{4.00\pm0.01}$ (hausmannite shows very small deviations from stoichiometry which is below the detection limit of the titration); an accuracy of $O_{3.00\pm0.01}$, with respect to $LaMnO_3$, was achieved.

Magnetic properties of the products were measured with a Quantum Design MPMS SQUID magnetometer. Susceptibility measurements were performed with a field of 100 Oe on heating after cooling in zero-field (ZFC). The field dependence of the magnetization of polycristalline pellets was recorded at 5 K. Four-probe electrical resistance measurements were made on sintered pellets between 30 and 300 K in a four-probe device. Seebeck data were obtained with a home-built device between 30 and 300 K.

Results

1. Sample Preparation and X-ray Characterization. The nonstoichiometry δ of the samples of $La_{1-y}MnO_{3-(3y/2)+\delta}$ and $LaMn_{1-z}O_{3-(3z/2)+\delta}$ as determined by redox titration is summarized in Table 1 for different starting La/Mn ratios. The $\delta = 0$ compositions refer to those with Mn exclusively in the Mn^{3+} state.

Samples prepared at 1200 °C in air or Ar crystallize in the orthorhombic $GdFeO_3$ structure (*Pbnm*) at room temperature, but a ratio $c/a < \sqrt{2}$ signals a cooperative Jahn−Teller deformation of the O′-orthorhombic phase. Samples prepared at 800 °C have larger values of δ and the rhombohedral perovskite structure ($R\bar{3}c$) at room temperature. Figure 1 shows the lattice parameter variation with composition for the orthorhombic samples; a linear variation of the lattice constants with *y* or *z* (Vegard's law) is observed for $y, z < 0.10$, but the $y = 0.15$ sample clearly deviates from the extrapolated line for both air- and Ar-fired samples. Samples with $y, z < 0.10$ are single phase to X-ray powder diffraction, but

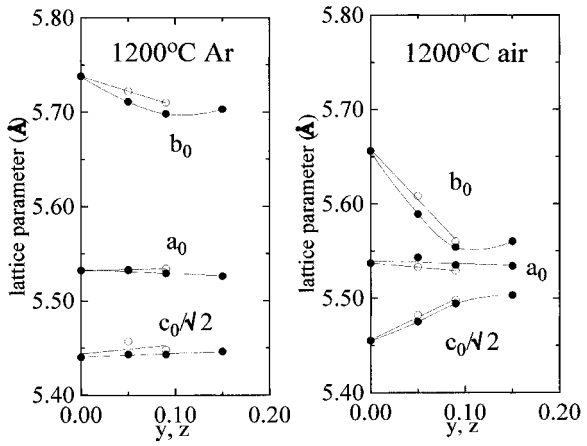

Figure 1. Variation of room-temperature cell parameters with y or z for $La_{1-y}MnO_{3-(3y/2)+\delta}$ (full circles) and $LaMn_{1-z}O_{3-(3z/2)+\delta}$ (empty circles) prepared at 1200 °C in Ar and air.

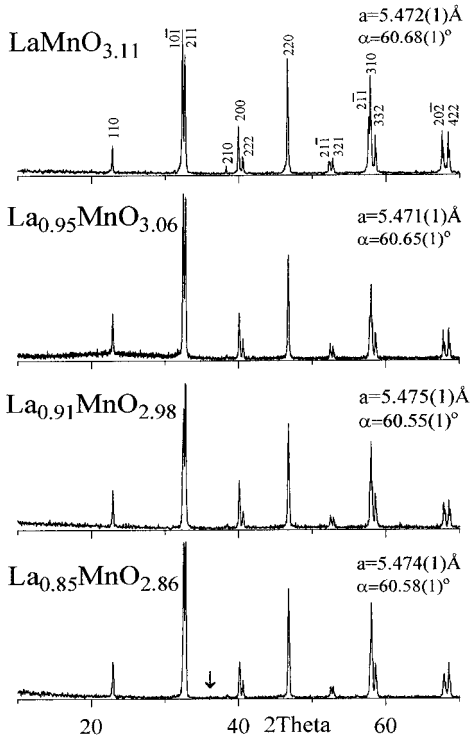

Figure 2. Room-temperature X-ray diffraction powder patterns (Cu Kα) for rhombohedral perovskites of the system $La_{1-y}MnO_{3-(3y/2)+\delta}$ prepared at 800 °C in oxygen; small impurity peaks (Mn_3O_4) in the case of $y = 0.15$ are marked by arrows.

the powder pattern for $y = 0.15$ shows weak reflections of Mn_3O_4 as a second phase. Figure 2 compares the X-ray powder patterns for the rhombohedral samples fired at 800 °C in oxygen; the position of the strongest reflection of hausmannite, Mn_3O_4, is indicated by an arrow. A monotonic decrease of the rhombohedral angle α is found for $y \leq 0.09$, but the $y = 0.15$ sample has a value too large for this trend and the powder pattern shows the presence of Mn_3O_4. These data indicate that the boundary of the single-phase field of the manganites $La_{1-y}MnO_{3-(3y/2)+\delta}$ is near $y = 0.10$ in good agreement with other studies on the composition of the perovskite phase field.[12,13] According to that, the thin film sample $La_{0.76}MnO_{2.73}$ [14] and the samples of $La_{1-y}MnO_{3-(3y/2)+\delta}$ with $y > 0.1$ from ref 15 are not within the perovskite stability field.

2. Magnetic Properties. Inverse magnetic susceptibility versus temperature curves (Figure 3a−e), indicate Curie−Weiss behavior with a Weiss temperature $\theta_p > 0$ that increases with δ. Samples with $0 \leq \delta \leq 0.05$ have a magnetic ordering temperature $T_c > \theta_p$; and $(T_c - \theta_p)$ decreases with y and δ. Samples with $0.10 \leq \delta \leq 0.15$ show typical ferromagnetic behavior with $T_c < \theta_p$ indicating short-range magnetic order above T_c. On the other hand, samples with the highest δ values, i.e., those prepared by direct heating at 800 °C in oxygen, have high values of T_c with the reappearance of a $T_c > \theta_p$. The effective magnetic moments μ_{eff} obtained from the slope of χ^{-1} vs T below 300 K (Table 1) are higher than calculated for spin-only moments on the Mn atoms.

Figure 4 shows the evolution of T_c with δ. Samples with $\delta \cong 0$ have a $T_c \approx 130$ K essentially independent of the La/Mn ratio, which was confirmed recently by another study.[16] Samples with La/Mn < 1 show a faster increase in T_c with δ than is found for $LaMnO_{3+\delta}$; those with La/Mn > 1 show a decrease with increasing δ in the range $0 \leq \delta \leq 0.15$, but an abrupt increase at highest δ. A $T_c = 250-270$ K is approached for all samples prepared by direct annealing at 800 °C, i.e., at highest δ values for a given system.

Figure 5 compares the molar magnetizations measured at 5 K in fields up to 40 kOe for $LaMnO_{3+\delta}$ (Figure 5a), $La_{0.91}MnO_{2.865\pm\delta}$ (Figure 5b), and $LaMn_{0.91}O_{2.865\pm\delta}$ (Figure 5c) for various values of δ. All samples with $\delta = 0$, i.e., with all Mn^{3+} ions, are antiferromagnetic with only a weak ferromagnetism due to spin canting by Dzialoshinskii antisymmetric exchange.[17] The magnetization increases with δ, approaching full ferromagnetic alignment of the spins (straight line at the top of the inset in Figure 5) in the range $0.10 \leq \delta \leq 0.14$ in $LaMnO_{3+\delta}$ and $La_{0.91}MnO_{2.865+\delta}$; significantly lower magnetizations are found at higher values of δ and in $LaMn_{0.91}O_{2.865+\delta}$.

3. Transport Properties. Measurements of the thermoelectric power as a function of temperature, α-(T), between 30 and 320 K are shown in Figure 6a−d. Figure 6a displays data for two representative samples with $\delta \cong 0$. A little oxidation of the Mn^{3+} is evident from the large, positive value of α(T); the oxygen partial pressure of the argon atmosphere used for the sample preparation was not low enough to achieve an ideal $\delta = 0$. The α(T) curves of orthorhombic samples prepared at 1200 °C (Figure 6b) are compared with those for rhombohedral samples prepared at 800 °C (Figure 6c). Samples with La/Mn > 1 have an $\alpha(T) \sim (k/e)\exp(E_\sigma/kT)$ typical of semiconductors; at low temperatures, the impedance was too high to allow measurements of α-(T). On the other hand, samples with La/Mn < 1 exhibit a maximum in α(T) at $T_{\alpha(max)}$ with a value α_{max} that decreases with increasing y; and below 100 K, α(T) drops to values close to 0 μV/K at larger y and/or δ. Above $T_{\alpha(max)}$, α(T) drops more gradually with T to a constant value if δ is maintained constant; but above room temperature, the oxygen content of the samples comes into equilibrium with the partial pressure of oxygen of the measuring atmosphere.[5]

Figure 6d shows the α(T) curves for samples with the highest δ, i.e., those prepared by direct heating at 800 °C in oxygen without preannealing at high temperatures. In this case, samples with La/Mn > 1 also display

(16) Hauback, B.; Fjellvag, H.; Sakai, N. *J. Solid State Chem.* **1996**, *124*, 43.
(17) Dzyaloshinskii, J. *J. Phys. Chem. Solids* **1958**, *4*, 241.

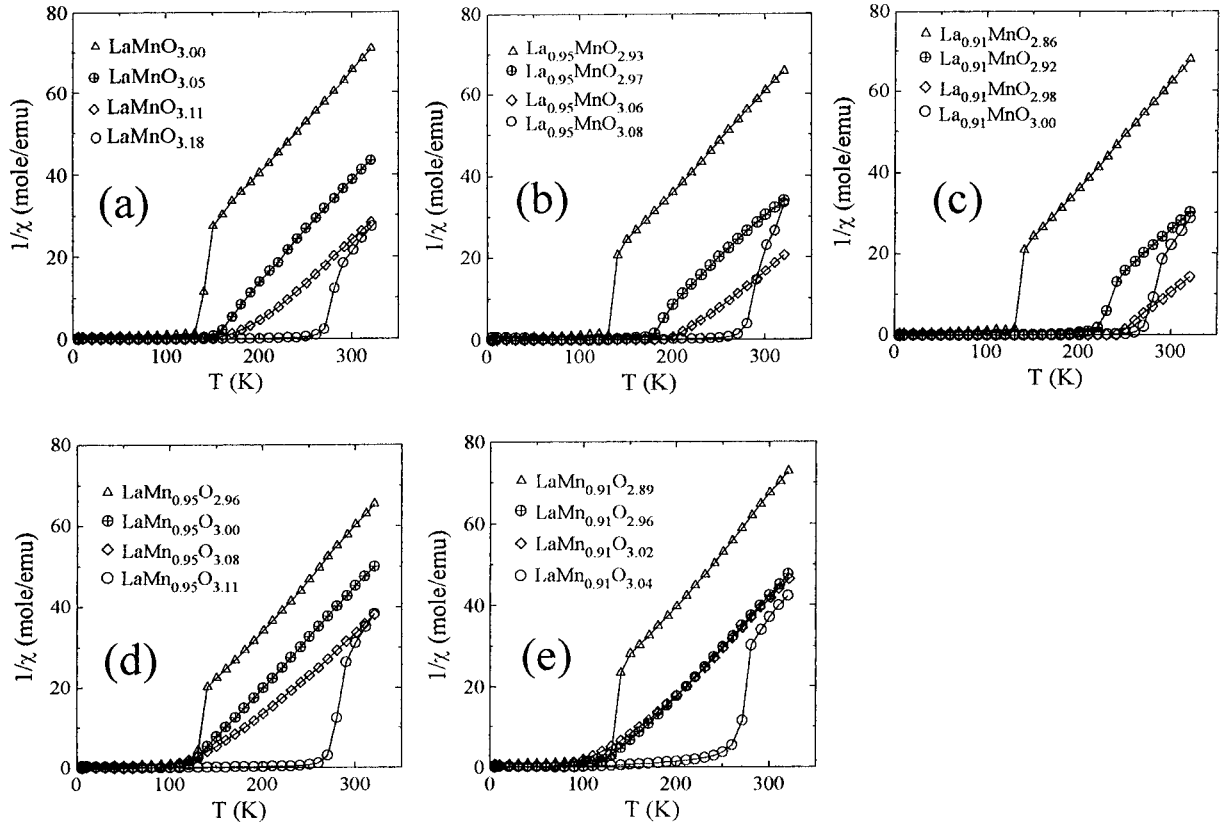

Figure 3. Temperature dependence of the inverse magnetic susceptibility measured in a field of 100 Oe for $LaMnO_{3+\delta}$ (a), $La_{0.95}MnO_{2.925+\delta}$ (b), $La_{0.91}MnO_{2.865+\delta}$ (c), $LaMn_{0.95}O_{2.925+\delta}$ (d), and $LaMn_{0.91}O_{2.865+\delta}$ (e).

an α_{max} at a $T_{\alpha(max)}$; α_{max} decreases and $T_{\alpha(max)}$ increases as the Mn deficiency decreases. The α_{max} and $T_{\alpha(max)}$ of La/Mn ≤ 1 samples are essentially independent of y over the range $0 \le y \le 0.09$.

The temperature dependence of the resistance $R(T)$, shown in Figure 7 for $La_{0.95}MnO_{2.925+\delta}$, is semiconducting at all temperatures for $\delta = 0.05$ (Figure 7a) but exhibits two maxima for $\delta = 0.14$ (Figure 7b) a sharp peak at T_c, and another broader peak at about 130 K. At $\delta = 0.16$, an enhanced broad peak retains the change at T_c only as a small shoulder. The corresponding $\alpha(T)$ curves and T_c are also shown. The data for $La_{0.91}MnO_{2.865+\delta}$ (Figure 8) show the two maxima in $R(T)$ superimposed on a semiconducting background in the $\delta = 0.06$ sample (Figure 8a) and an abrupt resistance drop on cooling through $T_c = 250$ K for $\delta = 0.12$ that is mimicked in the $\alpha(T)$ curve; but $\alpha(T)$ shows a second broad maximum below T_c whereas $R(T)$ shows a metallic behavior. The $\delta = 0.14$ sample (Figure 8c) shows a broad maximum in $R(T)$ at about 150 K, well below T_c, which is marked by a small shoulder in $R(T)$ near 260 K. The compounds with La/Mn > 1 tend to be all semiconductive (Figure 9); however, the sample with the highest δ for $z = 0.05$, $LaMn_{0.95}O_{3.11}$, shows a resistance maximum superimposed on a semiconductive background (Figure 9b).

Discussion

As previously noted in the literature,[12,13] the parent perovskite $LaMnO_3$ is able to display a large range of nonstoichiometry in both the La/Mn ratio and the oxygen content. Stoichiometric $LaMnO_3$ is attained at 1200 °C for oxygen activities of $-5 \le \log a_{O_2} \le -8$ and at 1000 °C for $-7 \le \log a_{O_2} \le -12$.[9,11] At higher oxygen activity, an oxygen-excess $LaMnO_{3+\delta}$ accommodates the

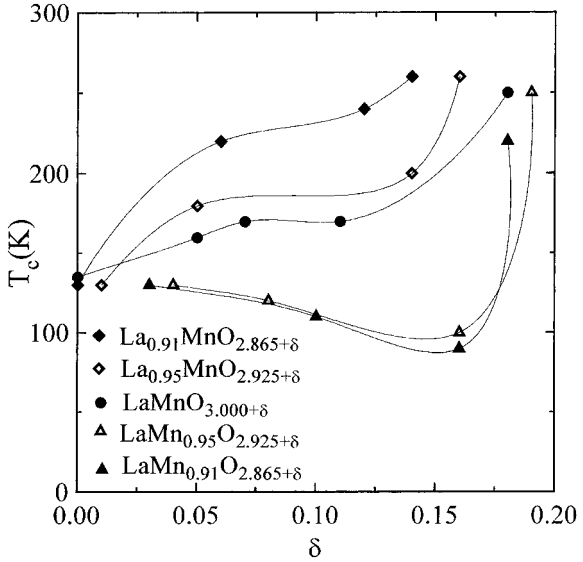

Figure 4. Variation of the magnetic ordering temperatures T_N or T_c with δ for the systems $La_{1-y}MnO_{3-(3y/2)+\delta}$ and $LaMn_{1-z}O_{3-(3z/2)+\delta}$.

excess oxygen by creating cation vacancies to give $La_{1-\epsilon}Mn_{1-\epsilon}O_3$ with $\epsilon = \delta/(3 + \delta)$. At lower oxygen activities, oxygen deficient $LaMnO_{3-\delta}$ is obtained.[9,11] In our experiments, we could investigate only the range of oxygen stoichiometry $\delta \ge 0$, where we define $\delta = 0$ to be the composition with all Mn^{3+} ions. Our oxygen activities were never low enough to access the Mn^{3+}/Mn^{2+} couple.

In compounds with La/Mn ≠ 1, the $\delta = 0$ composition has vacancies on the oxygen array as well as the cation-deficient array since the structure accommodates vacancies more readily than interstitial atoms. With increasing δ, the oxygen vacancies are first eliminated

to give $O_{3.00}$ before vacancies are created on the second cation array. In $La_{0.95}MnO_{2.925+\delta}$, for example, vacancies at both La sites and oxygen sites are present at $\delta = 0$; at $\delta \geq 0.075$ the oxygen positions are filled up and cation vacancies are found at both La and Mn positions in analogy to the system $LaMnO_{3+\delta}$. This scheme is reflected in the notation used in Table 1.

With or without vacancies, the structure of the perovskites are determined first by the relative equilibrium bond lengths. The bond-length mismatch in an AMO_3 perovskite is given by the Goldschmidt tolerance factor

$$t = (A-O)/\sqrt{2}(B-O) \qquad (2)$$

where (A−O) is the mean equilibrium bond length for the ions occupying A sites and (M−O) for the ions on M sites. In ionic crystals with localized d^n configurations at any transition-metal atom M, the room-temperature (M−O) and (A−O) at ambient pressure may be calculated from the sums of the empirical ionic radii, and a $t < 1$ is found for $LaMnO_3$. A $t < 1$ may be accommodated by a cooperative rotation of the MO_6 octahedra about a [110] axis to give the orthorhombic (*Pbnm*) structure of $GdFeO_3$. As t increases toward unity, cooperative rotations of the oxygen atoms about a [111] axis give the rhombohedral ($R\bar{3}c$) symmetry of $LaAlO_3$.

In $LaMnO_3$, the octahedral-site Mn^{3+} ions have a localized d^4 configuration that, in cubic symmetry, is the orbitally 2-fold-degenerate t^3e^1, ^5E_g configuration. A cooperative Jahn−Teller deformation that removes the orbital degeneracy leaves the orthorhombic space group *Pbnm*, but this O′-orthorhombic phase is distinguished from the O-orthorhombic phase by a $c/a < \sqrt{2}$. Ordering of the localized, occupied e orbitals results in type-A antiferromagnetic order in which ferromagnetic $a-b$ planes are coupled antiparallel to nearest neighbor $a-b$ planes along the c-axis.[18,19] In $LaMnO_{3+\delta}$, a rhombohedral $R\bar{3}c$ symmetry is stable at room temperature in the range $0.10 \leq \delta \leq 0.16$.[5] In the rhombohedral phase, the e orbitals are constrained to be degenerate, which suppresses any static, cooperative Jahn−Teller deformation. Below room-temperature, there may be a transition to the O-orthorhombic phase,[7] but any Jahn−Teller deformations are either noncooperative or dynamic. The room-temperature O′-orthorhombic versus rhombohedral structures found in this study are presented in Table 1.

Discussion of the magnetic and transport properties for the perovskites with La/Mn ≠ 1 are best made in the context of those found for $LaMnO_{3+\delta}$. Therefore we begin with a brief summary of our conclusions[5] reached in the study of $LaMnO_{3+\delta}$.

In $LaMnO_{3.00}$ the cooperative Jahn−Teller distortion and the rules of superexchange lead to a type-A antiferromagnetic order. A weak ferromagnetic moment is caused by small canting of the antiferromagnetically ordered spins arising from Dzialoshinskij's antisymmetric exchange, the magnitude of that moment is about 0.4 μ_B in stoichiometric $LaMnO_3$.[16] As δ increases, the MnO_3 array is oxidized to give a mixed-valent Mn^{3+}/Mn^{4+} system. Trapping of Mn^{4+} ions at the cation vacancies introduces superparamagnetic clusters within which fast electron transfer from Mn^{3+} to Mn^{4+} ions introduces a ferromagnetic double exchange that is stronger than the antiferromagnetic $Mn^{3+}(t^1)-O:2p_\pi-Mn^{3+}(t^1)$ superexchange interactions. Ferromagnetic ordering within the clusters to form superparamagnetic regions may set in near room temperature. In the O′-

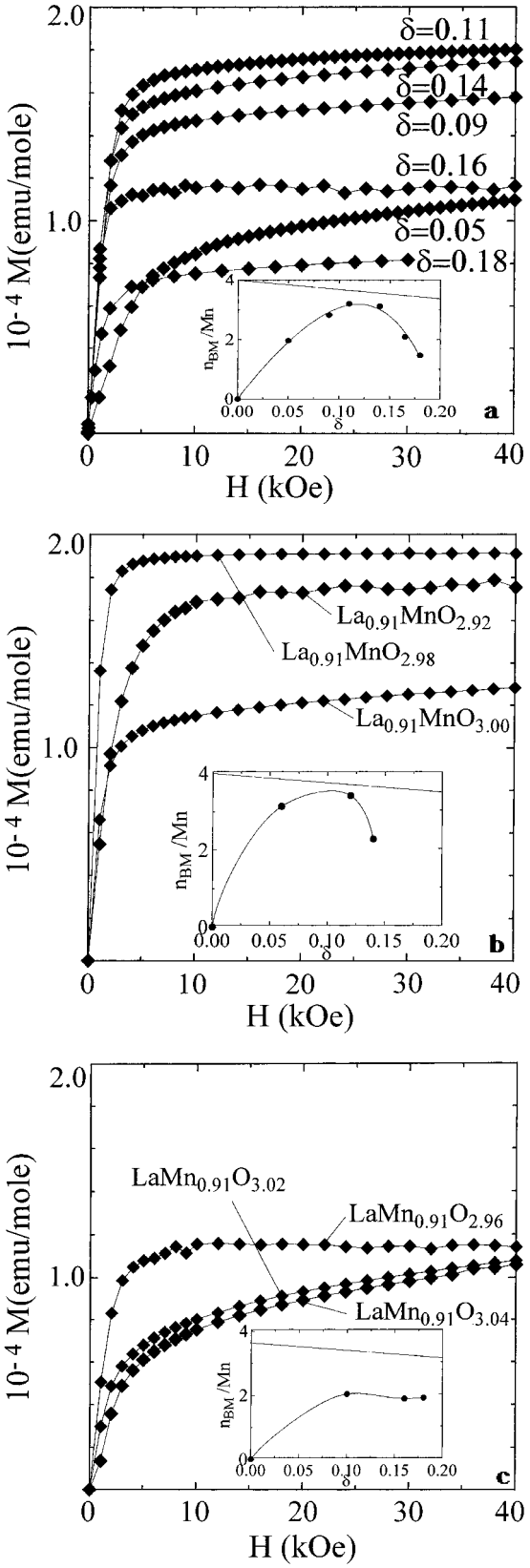

Figure 5. Field dependence of the molar magnetization at 5 K for the system $LaMnO_{3+\delta}$ (Figure 5a), $La_{0.91}MnO_{2.865+\delta}$ (Figure 5b), $LaMn_{0.91}O_{2.865+\delta}$ (Figure 5c); insets: variation of the number of moments at 5 K with δ (thin line at top: theoretical moments for full alignment of spins).

(18) Goodenough, J. B. *Phys. Rev.* **1955**, *100*, 564.
(19) Wollan, E. O.; Koehler, W. C. *Phys. Rev.* **1955**, *100*, 545.

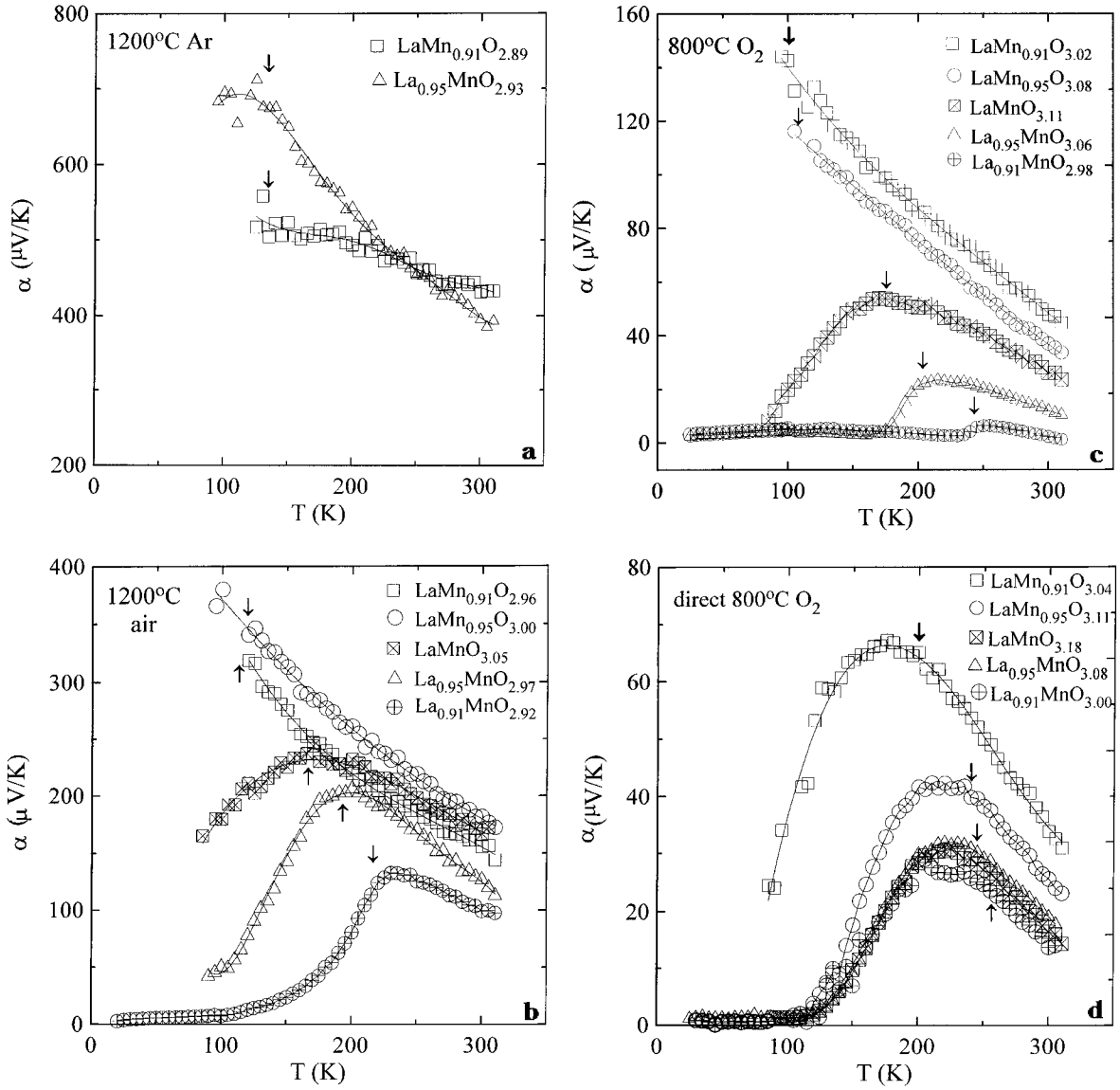

Figure 6. Variation of thermopower α with temperature for samples prepared at 1200 °C in Ar (Figure 6a), 1200 °C in air (Figure 6b), at 800 °C in oxygen (Figure 6c) and directly at 800 °C in oxygen (Figure 6d); T_c marked by vertical arrows.

orthorhombic phase, long-range coupling between randomly distributed clusters via an antiferromagnetic, hole-poor matrix is frustrated, which leads to spin-glass behavior below the ordering temperature T_c. The introduction of superparamagnetic clusters raises T_c from about 133 to 170−180 K.

The loss of a cooperative Jahn−Teller deformation in the rhombohedral phase introduces ferromagnetic coupling in the matrix. A dynamic correlation of half-filled and empty e orbitals on opposite sides of an oxygen atom via a dynamic Jahn−Teller coupling gives ferromagnetic Mn^{3+}−O−Mn^{3+} superexchange interactions.[20] Above T_c, the electron transfer from a Mn^{3+} to a Mn^{4+} ion remains polaronic, but the interaction remains ferromagnetic via superexchange. Below T_c, the Mn^{3+} to Mn^{4+} electron transfer is fast relative to the spin relaxation time at the Mn atoms, thereby stabilizing a double-exchange as against a superexchange ferromagnetic interaction via the e electrons within a fraction of the Mn−O−Mn linkages. The stronger double-exchange mechanism raises T_c at higher values of δ. Failure to reach a magnetization corresponding to full ferromagnetic alignment of all Mn spins was not clarified, but it appears to signal either retention of some antiferromagnetic domains in the range $0.10 \le \delta \le 0.14$ where a $T_c > \theta_p$ is found or retention of a small antiferromagnetic component in the matrix.

The ferromagnetic interaction via the e electrons must compete with the Mn(t^3)−O:$2p_\pi$−Mn(t^3) antiferromagnetic superexchange interactions. The strength of the ferromagnetic interactions increases with the width W_σ of the narrow σ^* band of e-orbital parentage in the absence of perturbations of the electronic potential, and

$$W_\sigma \approx \epsilon_\sigma \lambda_\sigma^2 \cos\phi \cos\theta_{ij} \qquad (3)$$

where $(180 - \phi)$ is the Mn−O−Mn bond angle and λ_σ is the Mn:e-O:$2p_\sigma$ covalent mixing parameter; θ_{ij} is the angle between the spins on neighboring Mn atoms. Oxidation of the MnO_3 array increases both λ_σ and cos ϕ, ferromagnetic ordering below T_c increases cos θ_{ij}. Above a critical bandwidth, there is a transition from polaronic to fast electron transfer from a Mn^{3+} to a Mn^{4+} ion. Oxidation of the MnO_3 array also suppresses the cooperative Jahn−Teller distortion by lowering the Mn^{3+} ion concentration. In the O′-orthorhombic phase, electron transfer from a Mn^{3+} to a Mn^{4+} ion remains

(20) Goodenough, J. B.; Wold, A.; Arnott, R. J.; Menyuk, N. *Phys. Rev.* **1961**, *124*, 373.

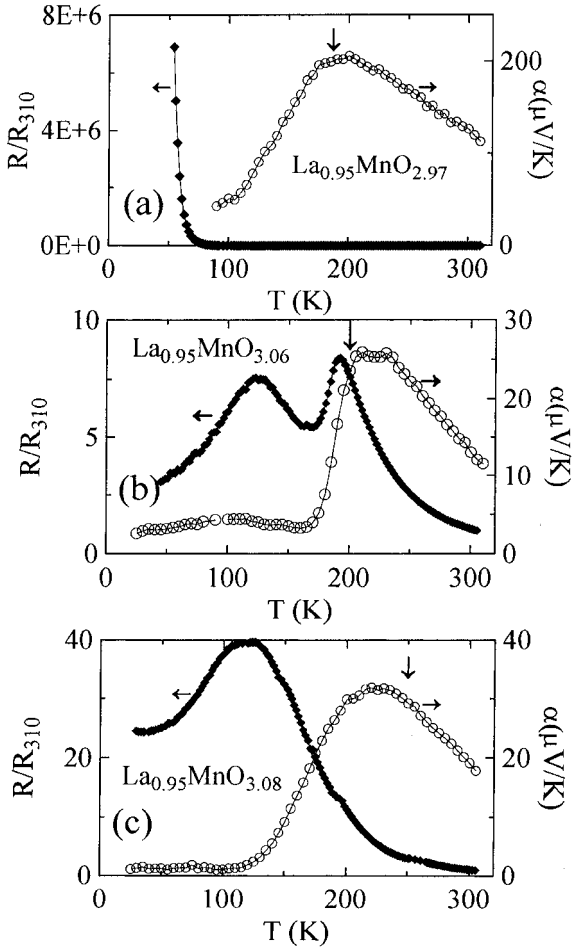

Figure 7. Temperature dependence of the electrical resistance normalized to the room-temperature resistance and the thermopower between 30 and 310 K for the system $La_{0.95}MnO_{2.925+\delta}$: $La_{0.95}MnO_{2.97}$ (a); $La_{0.95}MnO_{3.06}$ (b); $La_{0.95}MnO_{3.08}$ (c); T_c marked by vertical arrows.

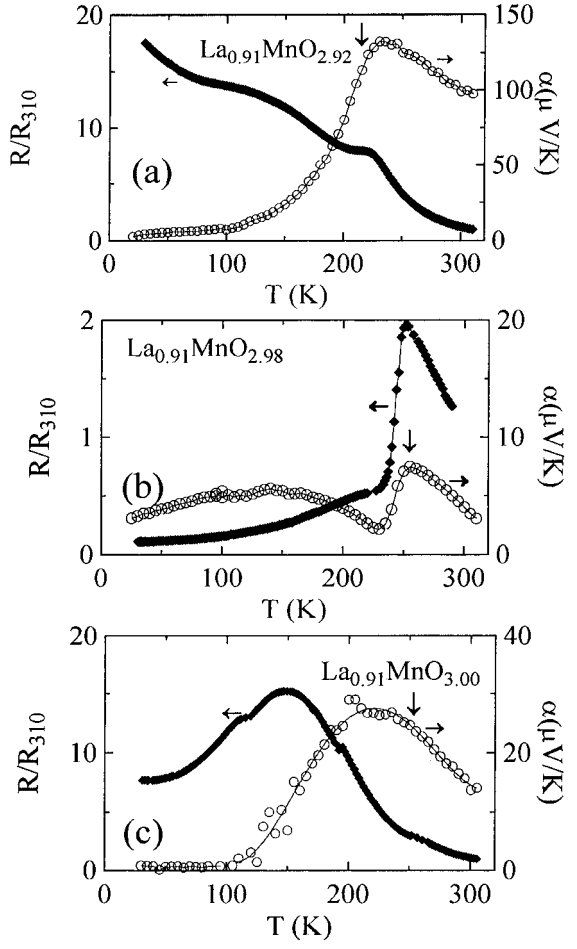

Figure 8. Temperature dependence of the electrical resistance normalized to the room-temperature resistance and the thermopower between 30 and 310 K for the system $La_{0.91}MnO_{2.865+\delta}$: $La_{0.91}MnO_{2.92}$ (a); $La_{0.91}MnO_{2.98}$ (b); $La_{0.91}MnO_{3.00}$ (c); T_c marked by vertical arrows.

polaronic at all temperatures; but in the rhombohedral phase, ferromagnetic alignment of the matrix below T_c increases W_σ to beyond the critical value for the onset of double-exchange, i.e. the electron-transfer time $\tau_h \approx \hbar W_\sigma$ decreases from $\tau_h > \omega_R^{-1}$ to $\tau_h < \omega_R^{-1}$, where ω_R^{-1} is the period of the oxygen breathing mode that traps a hole at an identifyable Mn^{4+} ion. A transition from $W_\sigma < \omega_R\hbar$ above T_c to $W_\sigma > \omega_R\hbar$ below T_c introduces a sharp drop in resistance on cooling through T_c. However, the resistance change is not a conventional metal−semiconductor transition. It is apparent from the Seebeck data that mobile polaronic holes in a narrow σ^* band are increasingly trapped out on cooling to T_c, but below T_c a broadening of W_σ releases trapped holes on cooling. Such a behavior is what would be expected where atomic vacancies perturb the electronic potential of the MnO_3 array so as to create Anderson localized states above a mobility edge near the top of the band.[21] The depth of the mobility edge μ_c into the band varies with the ratio of the perturbation energy to W_σ, so increasing W_σ below T_c can lower the Fermi energy from above μ_c to below it. However, below T_c the resistivity remains too high for a conventional metal, and a vanishing $\alpha(T)$ below 100 K signals that the conduction electrons are condensed into an unusual state. It has been suggested[22] that this state is a *vibronic* state associated with a strong coupling of the mobile holes to cooperative oxygen displacements along the Mn−O bond axes.

As δ increases, so does the Mn vacancy concentration, which perturbs more strongly the electron potential in the $Mn_{1-\epsilon}O_3$ array so as to increase the trapping out of Mn^{4+} ions. Clusters sufficiently rich in Mn^{4+} ions may become antiferromagnetic, thus lowering the net magnetization of the samples. Moreover, the antiferromagnetic clusters may induce the formation of ferromagnetic spiral-spin configurations in the matrix between them, especially where ferromagnetic double-exchange interactions varying as $\cos(\theta_{ij}/2)$ compete with antiferromagnetic $Mn^{3+}(t^3)$−O:$2p_\pi$−$Mn^{3+}(t^3)$ superexchange interactions varying as $\cos\theta_{ij}$.

It is from this perspective that we turn to an interpretation of the data presented here for systems with La/Mn ≠ 1. Similar to the system $LaMnO_{3+\delta}$, the perovskites with only Mn^{3+} ions ($\delta = 0$) order antiferromagnetically below about 130 K with a weak Dzialoshinskij ferromagnetic component. The existence of an O′-orthorhombic structure is consistent with type-A antiferromagnetic order stabilized by the same cooperative Jahn−Teller deformation found in $LaMnO_3$. The large, positive Seebeck coefficient (Figure 6a) shows that there are only a small number of mobile small-polaron holes in these materials.

In the samples with La/Mn < 1 ($y = 0.05$; $y = 0.09$), there are no Mn vacancies at lower values of δ, and the

(21) Mott, N. F.; Davis, E. A. *Electron processes in noncrystalline solids*, 2nd ed.; Oxford University Press: Oxford, 1979.
(22) Zhou, J. S.; Archibald, W.; Goodenough, J. B. *Nature* **1996**, *381*, 770.

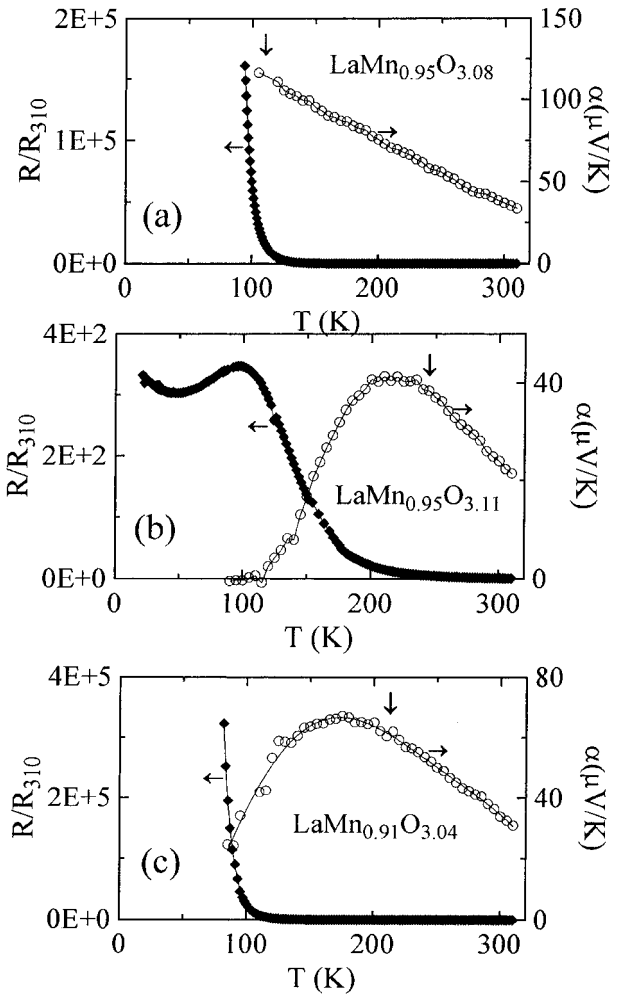

Figure 9. Temperature dependence of the electrical resistance normalized to the room-temperature resistance and the thermopower between 30 and 310 K for the system $LaMn_{1-z}O_{3-(3z/2)+\delta}$: $LaMn_{0.95}O_{3.08}$ (a); $LaMn_{0.95}O_{3.11}$ (b); $LaMn_{0.91}O_{3.04}$ (c); T_c marked by vertical arrows.

$MnO_{3-\delta}$ array is perturbed by oxygen vacancies, which trap Mn^{3+} ions, so the holes (Mn^{4+} ions) are more mobile than in $LaMnO_{3+\delta}$. The result is an increase in T_c relative to $LaMnO_{3+\delta}$ (Figure 4) and the realization of a ferromagnmetic matrix at a lower value of δ (Figure 5b vs 5a). Moreover, the $\alpha(T)$ curves of Figure 6b indicate less hole trapping above T_c (smaller α_{max}) and a more metallic behavior below T_c where there are no Mn vacancies (Figure 8b). However, introduction of Mn vacancies at larger δ (Figure 7b) appears to introduce a trapping out of holes below T_c (maximum in $R(T)$ at about 130 K) that are again released at lower temperatures with increasing ferromagnetic order. The broad maximum in $R(T)$ for the most oxidized samples (Figures 7c and 8c) appears to reflect the low density of the pellets; this feature is not reflected in the $\alpha(T)$ data.

In the samples with La/Mn > 1 ($z = 0.05$; $z = 0.09$), Mn vacancies are present at all values of δ, and the electron potential of the $Mn_{1-\epsilon}O_3$ array is more strongly perturbed than in $LaMnO_3$ for each value of δ. The result is a decrease in T_c relative to $LaMnO_{3+\delta}$ (Figure 4) and failure to reach a fully ferromagnetic sample at any value of δ (Figure 5c). Moreover, the $\alpha(T)$ data of Figure 6b,c show that holes continue to be trapped out to lowest temperatures (100 K); there is no α_{max} associated with the onset of ferromagnetic order, indicating no release of holes to the ferromagnetic matrix below T_c. Only at the highest δ values trapped holes are released to the matrix below T_c (Figure 6d); but this release is least where the Mn vacancies are present in highest concentration. The charge carriers remain polaronic; the maximum in $R(T)$ below T_c in Figure 9b, like that in Figures 7c and 8c, appears to reflect the low density of the pellets prepared by direct heating at 800 °C in oxygen atmosphere. We believe this $R(T)$ character is probably due to changes in the grain-boundary resistance.

The data of Figure 3 are consistent with this model. A $\mu_{eff} > \mu_{theory}$ signals either the presence of superparamagnetic clusters or a temperature-dependent Weiss molecular field. The increase in θ_p with δ, which is larger in the La/Mn < 1 samples than in $LaMnO_{3+\delta}$, is consistent with a smaller trapping out of the mobile holes; the opposite is found in the La/Mn > 1 samples where the holes are more strongly trapped and remain polaronic. However, the increase in T_c at highest values of δ for all samples coupled with a $T_c > \theta_p$ is remarkable. In these samples it appears that a first-order transition from polaronic to itinerant electronic behavior may occur at T_c within the matrix between clusters. In the itinerant electron regime, competition between a ferromagnetic double-exchange $\cos(\theta_{ij}/2)$ and an antiferromagnetic $t^3-p_\pi-t^3$ superexchange $\cos\theta_{ij}$ term may stabilize spin canting, lowering the magnetization and favoring the stabilizing of helical-spin configurations.

In conclusion, this systematic study of the variation of the transport and magnetic properties with the deviation from stoichiometry, δ, in nonstoichiometric manganese oxides with the perovskite structure extend the data obtained for $LaMnO_{3+\delta}$. They support the general picture developed for this system as well as for the doped, stoichiometric perovskites $Ln_{1-x}A_xMnO_3$; and they reveal the importance not only of the bandwidth W_σ but also of hole trapping in the vincinity of Mn vacancies in a $Mn_{1-\epsilon}O_3$ array. Although the systems are single phase crystallographically, the magnetic and electronic properties are clearly heterogeneous. These findings have recently been confirmed by high-resolution electron microscopy.[15] The authors report on grain-boundary near regions of possibly cubic structure with a diameter of about 400 Å in a rhombohedral sample with $y = 0.1$ appearing single phase according to XRD experiments.

After submission of this article we received a paper focused on the crystal structure of $La_{0.90}MnO_{2.85+\delta}$ with different values of δ.[23] Although the authors have found a monoclinic unit cell for $\delta \approx 0.10$ (our notation of δ) by X-ray diffraction, our samples of $La_{0.91}MnO_{2.865+\delta}$ with $\delta = 0.12$ and 0.14 could be completely indexed based on a rhombohedral cell.

Acknowledgment. J.T. would like to thank the German Academic Exchange Service (DAAD) for a scholarship; financial support of the NSF is also acknowledged.

CM9700211

(23) Maignan, A.; Michel, C.; Hervieu, M.; Raveau, B. *Solid State Commun.* **1997**, *101*, 277.